ORIGINAL RESEARCH

Numerical investigations of flat punch molding using a higher order strain gradient plasticity theory

Suman Guha · Sandeep Sangal · Sumit Basu

Abstract In this work we have revisited the problem of molding a deformable substrate with a rigid flat punch. The work is motivated by the recent experiments by Chen et al. (Acta Mater 59:1112−1120, 2011) where it was shown that systematically determined characteristic molding pressure H increased significantly with decrease in punch width, for widths less than ~ 25 μm. This size effect, akin to the indentation size effect observed in nano-indentation of metals, assumes importance in applications involving molding of metallic microstructures. Numerical simulations have been conducted within the framework of a finite deformation higher order strain gradient model. While classical plasticity predicts almost uniform stress with severe plastic strain concentration at the sharp corners to prevail just beneath the punch, our simulations present a significantly different picture. Very narrow punches have fairly uniform plastic strain with severe concentration of strain gradients and large contact stresses close to the edges. Wider punches however, behave in a manner closely resembling the predictions of classical plasticity.

S. Guha · S. Sangal
Department of Materials Science and Engineering,
Indian Institute of Technology Kanpur, Kanpur 208016,
Uttar Pradesh, India

S. Guha
e-mail: gsuman@iitk.ac.in

S. Sangal
e-mail: sangals@iitk.ac.in

S. Basu (✉)
Department of Mechanical Engineering, Indian Institute
of Technology Kanpur, Kanpur 208016,
Uttar Pradesh, India
e-mail: sbasu@iitk.ac.in

Introduction

The problem of a flat punch indenting a deformable elasto-plastic half space (shown in Fig. 1) is one of the most well-studied problems in mechanics. Hill's [2] slip-line field solution for a rigid perfectly plastic half space yields the simple solution that the pressure beneath the indenter is a constant and is given by

$$\frac{H}{\sigma_0} = \frac{2 + \pi}{\sqrt{3}}, \tag{1}$$

where σ_0 is the yield stress of the material. Unlike indentation with wedges or cylinders, flat punch indentation is not self similar and the deformation evolves with the depth of indentation h. In spite of this complication, the above estimate of H seems to be a rather good one. In fact, Nepershin [3] has shown that the slip line field solution is very accurate for $h/2w \geq 8$, where $2w$ is the punch width. Moreover, Finite Element (FE) analysis of the problem (see [4]) using a strain hardening elasto-plastic material has confirmed that beyond the elastic regime (during which H increases linearly with h) H is a weakly increasing function of $h/2w$ with a value that is close to what is given by Eq. 1. Recently (see [5]), the slip line field solution has been verified experimentally through particle image velocimetry. Especially striking was the visualization of a 'dead metal zone' right beneath the indenter with width equal to $2w$, where the metal was pushed downwards at the same velocity as the indenter.
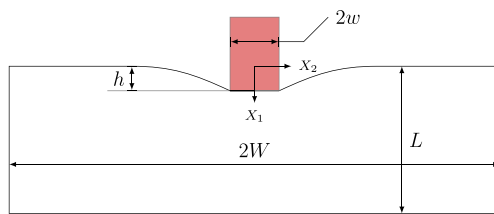
Fig. 1 Schematic of the flat punch molding

In recent years, attempts have been made to fabricate metal based microscale structures with characteristic feature sizes of tens of microns [6–8]. Metal based microscale structures are attractive in applications like micro-electromagnetics and microscale heat exchanger devices. An attractive route to rapid mass production of such microscale structures is the LiGA protocol [9]. In this protocol, a primary microscale mold insert is fabricated by combining deep lithography and electrodeposition. Secondary structures are then generated repetitively from the primary insert by compression molding. The process has been successfully applied to transfer the pattern on the insert with high fidelity to thin polymeric films (see, for example [10]). However, Cao et al. [6] and Cao and Meng [7] have successfully used this technique to compression mold high aspect ratio metallic microscale structures onto Pb, Zn and Al using specially surface treated Ni inserts.

The problem of the flat punch indenting a semi infinite substrate assumes renewed importance in the light of the above developments. However, now we have to contend with the fact that in the micro molding process, the punch width $2w$ may be extremely small and size dependent plasticity models like the mechanism based and higher order strain gradient theories of Nix and Gao [11] and Fleck and Hutchinson [12, 13] respectively are more appropriate than classical ones. It is indeed the case that while indenting a material with indenters of self-similar geometries like cones or spheres, the measured hardness turns out to be much higher at small depths of indentation for cones (see [11]) and small radii for spheres [14]—facts that have been called the indentation size effect (ISE).

Studies of microscale molding with flat punches has been made by Jiang et al. [8] and Chen et al. [1]. In the former, it has been shown that for punch widths larger than 150 μm, the molding response of Al is almost size independent. However, the latter work extends this to even smaller punch widths (of the order of 25 μm and lower) and shows that the characteristic pressure under the punch increases significantly with decrease in $2w$ below ~ 10 μm. Like in the case of ISE, the explanation to this phenomenon is based on the concept of geometrically necessary dislocations (GND) which have to be present near the punch in order to accommodate the volume of the material displaced by it. Evidently, when feature sizes as small as 1 μm are

being attempted, a reliable estimate of $H(w)$ is needed to predict the molding loads.

In this work, numerical simulations are used to understand the size dependence of the molding pressure observed by Chen et al. [1]. To this end, we use a formulation for plasticity at small scales provided by the strain gradient plasticity model originally proposed by Fleck and Hutchinson [12] and subsequently reformulated [13] to a framework that is more suitable for numerical applications and closer in spirit to the early models of Aifantis [15]. The mathematical structure of strain gradient based models is different from the Nix and Gao [11] model in the sense that more boundary conditions compared to conventional theories of plasticity need to be specified. As a result, the theory can capture boundary layer phenomenon related to surfaces and interfaces. These theories aspire to provide a framework for a large gamut of problems where a size effect manifests eg. nano-indentation, bending of thin beams [16] and torsion of fine wires [17]. We use a large deformation based Finite Element (FE) implementation of the viscoplastic version [18] of the reformulated [13] model to capture the effect of punch size w on the molding pressure.

Material model

Basic kinematics

The displacement of a point in space is denoted as,

$$u_i = x_i - X_i, \tag{2}$$

where X_i is a material point and x_i is the position of the same in the deformed configuration. The deformation gradient tensor and the velocity gradient tensor are given in the conventional manner as

$$F_{ij} = \frac{\partial x_i}{\partial X_j} \text{ and} \tag{3}$$

$$L_{ij} = \frac{\partial \dot{u}_i}{\partial x_j} = \dot{u}_{i,j}. \tag{4}$$

The strain rate is derived from the symmetric part of L_{ij} as

$$\dot{\epsilon}_{ij} = \frac{1}{2} \left(L_{ij} + L_{ji} \right). \tag{5}$$

Further $\dot{\epsilon}_{ij}$ is decomposed additively into the elastic and the plastic part as

$$\dot{\epsilon}_{ij} = \dot{\epsilon}_{ij}^e + \dot{\epsilon}_{ij}^p. \tag{6}$$

The skew-symmetric part of the velocity gradient tensor is

$$\dot{\omega}_{ij} = \frac{1}{2} \left(L_{ij} - L_{ji} \right). \tag{7}$$

It is also assumed that the material follows von-Mises material behavior and the normality rule holds true under the present formulation, which implies,

$$\dot{\epsilon}_{ij}^p = \frac{3\sigma_{ij}'}{2\sigma_e}\dot{\epsilon}^p = m_{ij}\dot{\epsilon}^p, \tag{8}$$

where $\dot{\epsilon}^p$ is the equivalent plastic strain defined as $\sqrt{2\dot{\epsilon}_{ij}^p\dot{\epsilon}_{ij}^p/3}$ and σ_{ij}' is the deviatoric part of the stress tensor. The tensor $m_{ij} = 3\sigma_{ij}'/2\sigma_e$ is defined in terms of the equivalent stress $\sigma_e = \sqrt{3\sigma_{ij}'\sigma_{ij}'/2}$. In order to incorporate non-local effects due to strain gradient following [13], an effective plastic strain rate is defined in terms of the plastic strain rate and the gradient of plastic strain rate as

$$\dot{E}^{p2} = \dot{\epsilon}^{p2} + l_*^2\dot{\epsilon}_{,i}^p\dot{\epsilon}_{,i}^p, \tag{9}$$

where l_* is the characteristic length scale of the material introduced to maintain dimensional consistency.

Virtual work relation and material model

Under the framework of gradient plasticity the conventional virtual work relation is augmented by the virtual work corresponding to the gradient of plastic strain and its work conjugate, a higher order stress quantity. According to [19] the virtual work relationship for a gradient plastic material is given as

$$\int_V \left(\sigma_{ij}\delta\dot{\epsilon}_{ij}^e + Q\delta\dot{\epsilon}^p + \tau_i\delta\dot{\epsilon}_{,i}^p\right)dV = \int_S \left(T_i\delta\dot{u}_i + t\delta\dot{\epsilon}^p\right)dS, \tag{10}$$

where left hand side of Eq. 10 corresponds to the internal virtual work and the right hand side, the external virtual work. Here, $\sigma_{ij}\delta\dot{\epsilon}_{ij}^e$ represents the virtual work due the elastic strain increment and Q is a scalar microstress which contributes to the virtual work due to the plastic strain increment. Additionally, τ_i is the higher order stress, work conjugate to the virtual incremental quantity $\delta\dot{\epsilon}_{,i}^p$ (the gradient of plastic strain). The above virtual work relation is different from the corresponding conventional equation in a sense that both the displacement and the equivalent plastic strain are considered to be independent kinematic quantities. As a consequence of the above consideration additional boundary conditions on $\dot{\epsilon}^p$ or on the higher order tractions need to be imposed. The right hand side of Eq. 10 hence represents the external virtual work by the conventional tractions and the external virtual work due to higher-order tractions. The equilibrium equations and the boundary conditions can be obtained from Eq. 10 by the application of the Gauss' theorem and noting that Eq. 10 holds true for any arbitrary variations of $\dot{u}_i$ and $\dot{\epsilon}^p$. The equilibrium equations

consist of the conventional equilibrium equation $\sigma_{ji,j} = 0$, with an additional consistency condition given by,

$$Q = \sigma_e + \tau_{i,i}. \tag{11}$$

The boundary conditions are,

$$T_i = \sigma_{ji}n_j, \text{ and} \tag{12}$$
$$t = \tau_i n_i, \tag{13}$$

where n_i is the unit normal to the surface where the boundary tractions T_i or the higher order tractions t are specified. Additionally boundary conditions of the form,

$$u_i = u_i^* \text{ and} \tag{14}$$
$$\epsilon^p = \epsilon^{p*}, \tag{15}$$

on some parts of the boundary may be prescribed. Here, u_i^* and ϵ^{p*} are imposed displacement or equivalent plastic strain.

Updated Lagrangian framework

With a view to develop a finite deformation model under updated Lagrangian framework, the virtual work relation in Eq. 10 is now rewritten in the reference configuration following [19]. The Kirchhoff stress measures for various stress quantities are defined as,

$$\zeta_{ij} = J\sigma_{ij}, \tag{16}$$
$$\sigma_e^\zeta = J\sigma_e, \tag{17}$$
$$q = JQ, \text{ and} \tag{18}$$
$$\rho_i = J\tau_i. \tag{19}$$

Similarly, the first Piola–Kirchhoff stress measures are defined as,

$$s_{ij} = JF_{ik}^{-1}\sigma_{kj} = F_{ik}^{-1}\zeta_{kj}, \text{ and} \tag{20}$$
$$\varrho_i = JF_{ik}^{-1}\tau_k = F_{ik}^{-1}\rho_k, \tag{21}$$

where J is the determinant of the deformation gradient tensor. Using the above relations in Eq. 10, the virtual work equation in the reference configuration is obtained as follows,

$$\int_{V_0} \left(s_{ij}\delta\dot{F}_{ij} + \left(q - \sigma_e^\zeta\right)\delta\dot{\epsilon}^p + \varrho_i\delta\dot{\epsilon}_{,0i}^p\right)dV_0$$
$$= \int_{S_0} \left(T_{0i}\delta\dot{u}_i + t_0\delta\dot{\epsilon}^p\right)dS_0. \tag{22}$$

The incremental version of the above virtual work equation in the reference configuration becomes:

$$\int_{V_0} \left(\dot{s}_{ij}\delta\dot{F}_{ij} + \left(\dot{q} - \dot{\sigma}_e^\zeta\right)\delta\dot{\epsilon}^p + \dot{\varrho}_i\delta\dot{\epsilon}_{,0i}^p\right)dV_0$$
$$= \int_{S_0} \left(\dot{T}_{0i}\delta\dot{u}_i + \dot{t}_0\delta\dot{\epsilon}^p\right)dS_0. \tag{23}$$

As the constitutive relations will be formulated in terms of the Jaumann rate of Kirchhoff stress ($\overset{\triangledown}{\zeta}_{ij}$) and convected rate of the higher order Kirchhoff stress ($\overset{\vee}{\rho}_i$), [18] the following identities have been used under updated Lagrangian framework,

$$\overset{\triangledown}{s}_{ij} = \overset{\triangledown}{\zeta}_{ij} - \sigma_{kj}\dot{\epsilon}_{ik} - \sigma_{ik}\dot{\epsilon}_{jk} + \sigma_{ik}L_{jk}, \text{ and} \tag{24}$$

$$\dot{\varrho}_i = \overset{\vee}{\rho}_i. \tag{25}$$

As mentioned in [19], the convected rate for higher order stress vector is employed in stead of the Jaumann rate because using the latter to define the constitutive relation for higher order stress yields a non-symmetric stiffness matrix. Finally the virtual work relation in the reference configuration takes the following form:

$$\int_V \left(\overset{\triangledown}{\zeta}_{ij}\delta\dot{\epsilon}_{ij} - \sigma_{ij}\left(2\dot{\epsilon}_{ik}\delta\dot{\epsilon}_{kj} - L_{kj}\delta L_{ki}\right) \right.$$
$$\left. + \left(\dot{q} - \dot{\sigma}_e^\zeta\right)\delta\dot{\epsilon}^p + \overset{\vee}{\rho}_i\delta\dot{\epsilon}_{,0i}^p \right) dV$$
$$= \int_S \left(\dot{T}_{0i}\delta\dot{u}_i + \dot{i}_0\delta\dot{\epsilon}^p\right) dS - \frac{1}{\Delta t}[\text{Eqm Corr}], \tag{26}$$

where [Eqm Corr] is given by,

$$\text{Eqm Corr} = \int_V \left(\sigma_{ij}\delta\dot{\epsilon}_{ij} + (Q - \sigma_e)\delta\dot{\epsilon}^p + \tau_i\delta\dot{\epsilon}_{,0i}^p \right) dV$$
$$- \int_S \left(T_{0i}\delta\dot{u}_i + t_0\delta\dot{\epsilon}^p\right) dS, \tag{27}$$

and is required in order to prevent the solution from drifting with time from equilibrium for large strain problems.

Constitutive relations

In this section the constitutive relations are defined by following a viscoplastic material model as described in [18]. A viscoplastic potential Φ is defined which is a function of a generalized effective stress σ_c, which is work conjugate to the effective plastic strain rate $\dot{E}^p$. It is assumed that the higher order stress quantities are derivable from the viscoplastic potential in the following manner,

$$\sigma_c = \frac{\partial\Phi}{\partial\dot{E}^p},$$
$$q = \frac{\partial\Phi}{\partial\dot{\epsilon}^p} = \sigma_c\frac{\partial\dot{E}^p}{\partial\dot{\epsilon}^p}, \text{ and}$$
$$\rho_i = \frac{\partial\Phi}{\partial\dot{\epsilon}_{,i}^p} = \sigma_c\frac{\partial\dot{E}^p}{\partial\dot{\epsilon}_{,i}^p}. \tag{28}$$

Using Eqs. 9 and 28, the constitutive relations for a strain gradient viscoplastic material becomes,

$$q = \frac{\sigma_c}{\dot{E}^p}\dot{\epsilon}^p, \tag{29}$$

$$\rho_i = \frac{\sigma_c}{\dot{E}^p}l_*^2\dot{\epsilon}_{,i}^p, \text{ and} \tag{30}$$

$$\sigma_c^2 = q^2 + l_*^{-2}\rho_i\rho_i. \tag{31}$$

In case $l_* = 0$ (i.e. for a conventional material) σ_c reduces to q. The viscoplastic material behavior is modeled as,

$$\sigma_c = \sigma_0\left(1 + \frac{E^p}{\epsilon_0}\right)^{1/n}\left(\frac{\dot{E}^p}{\dot{\epsilon}_0}\right)^m, \tag{32}$$

where σ_0 is the initial yield strength of the material and $g(E^p) = \sigma_0\left(1 + E^p/\epsilon_0\right)^{1/n}$ describes the uniaxial strain hardening response of the material. The quantity n is the strain hardening exponent, m governs the strain rate sensitivity and $\dot{\epsilon}_0$ is the reference strain rate. When $\dot{E}^p$ is close to or less than $\dot{\epsilon}_0$, Eq. 32 exhibits rate-independent behavior as $\sigma_c \approx g(E^p)$. The strain at initial yield is $\epsilon_0 = \sigma_0/E$. It is to be noticed that the above material behavior incorporates E^p and $\dot{E}^p$ in the power law, instead of ϵ^p and $\dot{\epsilon}^p$.

The incremental constitutive relations for the above viscoplastic material model can be summarized as,

$$\overset{\triangledown}{\zeta}_{ij}\Delta t = R_{ijkl}\left(\Delta\epsilon_{kl} - m_{kl}\Delta\epsilon^p\right), \tag{33}$$

$$\dot{q}\Delta t = \frac{\sigma_c}{\dot{E}^p}\left((m-1)\frac{\dot{\epsilon}^p}{\dot{E}^p}\Delta\dot{E}^p + \Delta\dot{\epsilon}^p\right)$$
$$+ \left(\frac{\dot{E}^p}{\dot{\epsilon}_0}\right)^m\frac{dg}{dE^p}\dot{\epsilon}^p\Delta t, \text{ and} \tag{34}$$

$$\overset{\vee}{\rho}_i\Delta t = l_*^2\left(\frac{\sigma_c}{\dot{E}^p}\left((m-1)\frac{\dot{\epsilon}_{,i}^p}{\dot{E}^p}\Delta\dot{E}^p + \Delta\dot{\epsilon}_{,i}^p\right)\right.$$
$$\left. + \left(\frac{\dot{E}^p}{\dot{\epsilon}_0}\right)^m\frac{dg}{dE^p}\dot{\epsilon}_{,i}^p\Delta t\right). \tag{35}$$

The elasticity tensor R_{ijkl} is given by,

$$R_{ijkl} = \frac{E}{1+\nu}\left(\frac{1}{2}(\delta_{ik}\delta_{jl} + \delta_{il}\delta_{jk}) + \frac{\nu}{1-2\nu}\delta_{ij}\delta_{kl}\right), \tag{36}$$

and increment in the effective plastic strain rate using Eq. 9 is given by,

$$\Delta\dot{E}^p = \frac{\dot{\epsilon}^p}{\dot{E}^p}\Delta\dot{\epsilon}^p + \frac{l_*^2\dot{\epsilon}_{,i}^p}{\dot{E}^p}\Delta\dot{\epsilon}_{,i}^p. \tag{37}$$

Finite element formulation

For FE analyses, we use isoparametric quadratic triangular elements. In addition to the increment of displacement components Δu_i, increment of equivalent plastic strain rate $\Delta\dot{\epsilon}^p$ is also used as a degree of freedom for each node. Both the displacement increments and the increments of equivalent plastic strain rate are interpolated within the element

using quadratic functions in terms of their respective nodal components ΔD_N and $\Delta \dot{\epsilon}_N^p$ as,

$$\Delta u_i = \sum_{N=1}^{2k} N_i^N \Delta D_N, \text{ and} \tag{38}$$

$$\Delta \dot{\epsilon}^p = \sum_{N=1}^{k} M^N \Delta \dot{\epsilon}_N^p, \tag{39}$$

where N_i and M are the shape functions and $k = 6$ is the number of nodes used for interpolation. Accordingly from the above relations, increments in the velocity gradient and the strain tensor can be represented in terms of the nodal displacement increment as,

$$\Delta L_{ij} = \sum_{N=1}^{2k} N_{i,j}^N \Delta D_N, \text{ and} \tag{40}$$

$$\Delta \epsilon_{ij} = \sum_{N=1}^{k} E_{ij}^N \Delta D_N, \text{ where,}$$

$$E_{ij} = \frac{1}{2} \left(N_{i,j}^N + N_{j,i}^N \right). \tag{41}$$

In a similar manner, the gradient of equivalent plastic strain rate is given by,

$$\Delta \dot{\epsilon}_{,i}^p = \sum_{N=1}^{k} M_{,i}^N \Delta \dot{\epsilon}_N^p. \tag{42}$$

Finally the virtual work relation is discretized using the above relations and can be expressed in the following form:

$$\begin{bmatrix} K_e & 0 \\ K_{ep} & K_p \end{bmatrix} \begin{bmatrix} \Delta D_N \\ \Delta \dot{\epsilon}_N^p \end{bmatrix} = \begin{bmatrix} \Delta F_1 \\ \Delta F_2 \end{bmatrix} + \begin{bmatrix} C_1 \\ C_2 \end{bmatrix}, \tag{43}$$

where the elastic stiffness matrix

$$K_e^{NM} = \int_V \left(E_{ij}^N R_{ijkl} E_{kl}^M \right. $$
$$\left. + \sigma_{ij} \left(N_{k,j}^M N_{k,i}^N - 2 E_{ik}^M E_{jk}^N \right) \right) dV, \tag{44}$$

the coupling matrix

$$K_{ep}^{NM} = -\int_V m_{ij} R_{ijkl} E_{kl}^M M^N dV, \tag{45}$$

and the plastic stiffness matrix

$$K_P^{NM} = \int_V \left(\left(\frac{\dot{\epsilon}^p}{\dot{E}^{p2}} (m-1) q + \frac{\sigma_c}{\dot{E}^p} \right) M^M M^N \right.$$
$$+ \frac{l_*^2 \dot{\epsilon}_{,i}^p}{\dot{E}^{p2}} (m-1) q M^M M_{,i}^N + \frac{\dot{\epsilon}^p}{\dot{E}^{p2}} (m-1) \rho_i M_{,i}^M M^N$$
$$\left. + \frac{l_*^2 \dot{\epsilon}_{,i}^p}{\dot{E}^{p2}} (m-1) \rho_k M_{,k}^M M_{,i}^N + \frac{l_*^2 \sigma_c}{\dot{E}^p} M_{,i}^M M_{,i}^N \right) dV, \tag{46}$$

need to be calculated for each element. The force vectors on the right of Eq. 43 are given by

$$\Delta F_1^N = \int_S \Delta T_i N_i^N dS + \Delta t \int_V E_{ij}^N R_{ijkl} m_{kl} \dot{\epsilon}^p dV, \tag{47}$$

where the conventional force vector is augmented by a volume force contribution from Eq. 33. The force vector corresponding to the higher order traction is given by,

$$\Delta F_2^N = \int_S \Delta \rho_i n_i M^N dS$$
$$- \Delta t \int_V \left(\left(m_{ij} R_{ijkl} m_{kl} \dot{\epsilon}^p + \dot{\epsilon}^p \frac{dg}{dE^p} \left(\frac{\dot{E}^p}{\dot{\epsilon}_0} \right)^m \right) M^N \right.$$
$$\left. + l_*^2 \dot{\epsilon}_{,i}^p \frac{dg}{dE^p} \left(\frac{\dot{E}^p}{\dot{\epsilon}_0} \right)^m M_{,i}^N \right) dV. \tag{48}$$

Further the force vectors corresponding to the equilibrium correction terms are

$$C_1^N = -\int_V \sigma_{ij} E_{ij}^N dV + \int_S T_i N_i^N dS, \text{ and} \tag{49}$$

$$C_2^N = -\int_V \left((Q - \sigma_e) M^N + \tau_i M_{,i}^N \right) dV$$
$$+ \int_S t M^N dS. \tag{50}$$

It can be observed that the system of equations in Eq. 43 are decoupled, in the sense that once ΔD_N is solved, $\Delta \dot{\epsilon}_N^p$ can be obtained using ΔD_N.

Six noded triangular elements with three Gauss integration points have been used in all the simulations reported here. Though stress oscillations have been reported for these elements by [20], we note that the present structure of the FE equations in Eq. 43 is significantly different from those dealt with by [20] or [19]. We obtained consistent results with these elements and no stress locking was noted.

However, as observed by [21], the use of C_2^N in simulations lead to numerical problems and therefore, $C_2^N = 0$ has been assumed.

We have used a viscoplasticity model for the numerical stability that it offers. A small value for $m = 0.04$ has been chosen which produces a rate-independent limit of the uniaxial response.

After the displacement increments and the plastic strain rate increments are solved, the various stress rates can be updated using the constitutive relations in Eqs. 34–35. The increments of Cauchy stress tensor and the higher order stress vector are calculated from the Jaumann rate of Kirchhoff stress tensor and the convective rate of higher order stress vector respectively according to,

$$\Delta \sigma_{ij} = \overset{\triangledown}{\zeta}_{ij} \Delta t + \Delta \omega_{ik} \sigma_{kj} + \sigma_{ik} \omega_{jk} - \sigma_{ij} \Delta \epsilon_{kk}, \text{ and} \tag{51}$$

$$\Delta \tau_i = \overset{\vee}{\rho}_i \Delta t + \Delta L_{ik} \tau_k - \tau_i \Delta \epsilon_{kk}. \tag{52}$$

Table 1 Values of the material paramaters used for the analysis

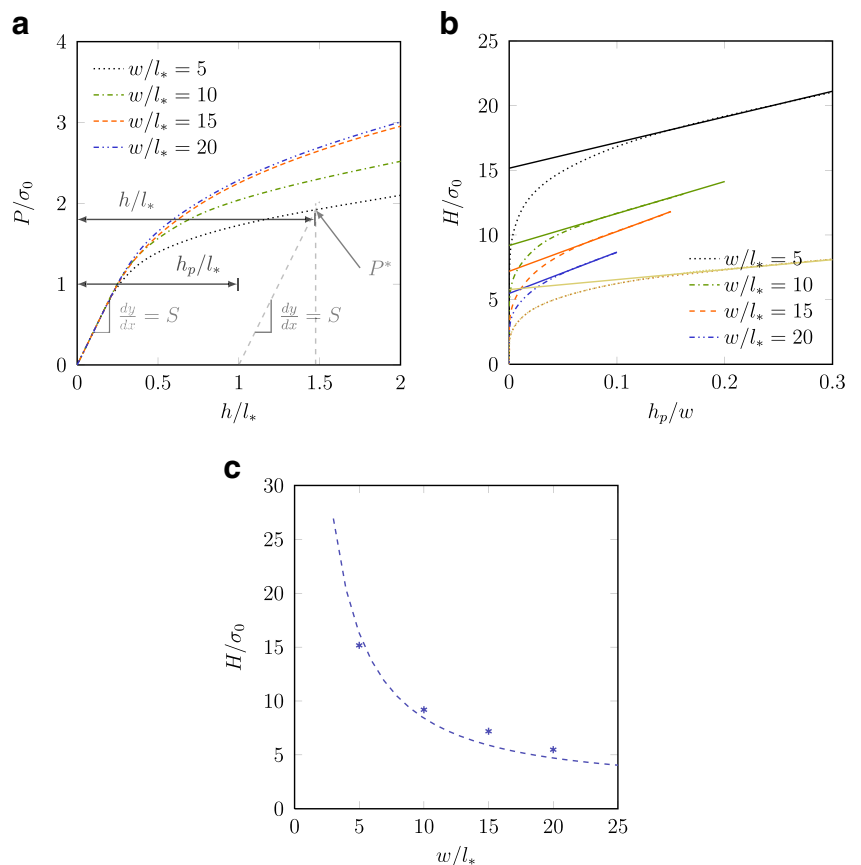| Reference strain	Strain hardening parameter	Reference strain rate	Strain rate sensitivity parameter
ϵ_0	n	$\dot{\epsilon}_0$	m
0.001	5	0.005	0.04

Further effective stress, σ_c is obtained from Eq. 31 and thereafter the equivalent plastic strain rate, $\dot{\epsilon}^p$ and its gradient, $\dot{\epsilon}^p_{,i}$ is obtained from Eqs. 29–30.

All material parameters used in this work are listed in Table 1.

Results and discussions

In the analysis reported in this section, the length scale parameter l_* has been used to normalize all distances. The absolute value of this parameter has been determined for a number of materials (see, [22]) and ranges from $\sim 1\ \mu m$ for superalloys to $\sim 10\ \mu m$ for Ni. It should be noted however that, it is still unclear if l_* is a material parameter or is dependent on the problem geometry.

Chen et al. [1] has followed a systematic procedure for determining the characteristic molding pressure from their experiments. We have followed the same procedure and it is explained in Fig. 2a–c. The normalized total load on the punch P/σ_0 for different values of the normalized punch width w/l_* used is plotted against the normalized depth h/l_* in Fig. 2a. The total load P experienced by the flat punch is evaluated as,

$$P(h) = \int_{-W}^{W} \sigma_{11}(x_2, h)dx_2, \tag{53}$$

where σ_{ij} is the Cauchy stress. Additionally, the part of the surface (S) in contact with the flat punch is subjected to the following boundary condition,

$$\dot{u}_1 = -\dot{h}, \text{ on S}, \tag{54}$$

$\dot{h}$ being the constant downward velocity at which the punch is pushed into the substrate. A very low rate of loading $\dot{h} = 0.005 l_* \text{s}^{-1}$ has been used. The punch is assumed to be frictionless in this work.

A sufficiently fine mesh has been used, especially close to the region where the corner of the flat punch makes contact with the substrate, with smallest elements having $\approx 0.04 l_*$ long sides.

Fig. 2 a Variation of total load with the depth experienced by the flat punch, for punches with various widths. **b** Plot of pressure $P/w\sigma_0$ under the punch with h_p/w for various punch width. The curves represented by the dotted lines corresponds to the same for conventional plastic material for two different punch widths. The curves for conventional material collapses to one. **c** Variation of characteristics hardness with the characteristic length, i.e. punch width w for flat punch indenter

The plastic part of the depth of penetration h, namely h_p, gives the residual depth of the impression that will remain when the punch is withdrawn from depth h. This quantity has been calculated in the experiments by Chen et al. [1] in a manner that is shown in Fig. 2a. Here $h_p = h - P/S$, where S is the slope of the initial linear portion of the $P(h)$ curve. When $H(h_p) = P/2w\sigma_0$ is replotted against h_p/w (see, Fig. 2b), the small depth limit can be obtained by extrapolating the linear portion of the $H(h_p)$ plot to the vertical axis. The extrapolated quantity $H(h_p = 0)$ (which will be denoted as H in the subsequent discussion) is a measure of the characteristic pressure on the punch at the onset of plastic deformation beneath the punch and is akin to the estimate in Eq. 1. Moreover, $H(h_p = 0) = \sigma_0 H(h/w, w, n, m)$ for small w. Note that, according to classical plasticity theories, at any given h_p/w, the curves for all punch widths should collapse into a single curve as in the experiments of Jiang et al. [8] with wide punches with $2w > 150 \ \mu m$. Unlike Eq. 1, in the present case, the characteristic pressure is dependent on w/l_* since we have used a strain gradient plasticity theory to estimate it. The variation of H with w/l_* has been plotted in Fig. 2c where it is seen that even for $w \simeq 25l_*$, H is higher than what is predicted by Eq. 1 i.e. $H = 2.96\sigma_0$. The variation of H with w is remarkably similar to the experimental results of Chen et al. [1] which pertain to the molding of single crystal Al substrate with focused ion beam milled diamond punches.

The plastic zone underneath a wide flat punch has been reported by early FE analyses of the problem (see, for example [4, 23]). The plastic zones obtained from conventional plasticity have been shown in Fig. 3a and b at two depths. Note that these solutions are independent of w. Plasticity initiates and is the most severe at the sharp corners of the punch. Till the bands of plasticity reaches the symmetry line $X_2 = 0$, the plastic zone develops in a non self-similar manner. Only after attaining the situation shown in Fig. 3b (pertaining to $h/w = 0.5$) does it start moving downwards with the punch in a self similar manner. The triangular shaped 'dead zone' at smaller values of depth is reminiscent of the classical slip line field solutions of the problem (see e.g., [4, 24]). The plastic zones in the case of the strain gradient material depend strongly on the punch width. For the narrow punch (Fig. 3c), the plastic strain concentration at the corner is very weak. On the other hand, for $w/l_* = 20$, the plastic zone closely resembles the conventional case. In other words, the narrower punch has a more uniform distribution of ϵ^p beneath the punch compared to the wider punch, for the same h/w.

This is further illustrated in Fig. 4 which shows the variation of ϵ^p with X_2/w (at $X_1/w = 0$) for the two punches at an early stage of the deformation. For comparison, the same variation obtained from classical size-independent plasticity analysis is also shown in the figure. Expectedly, the
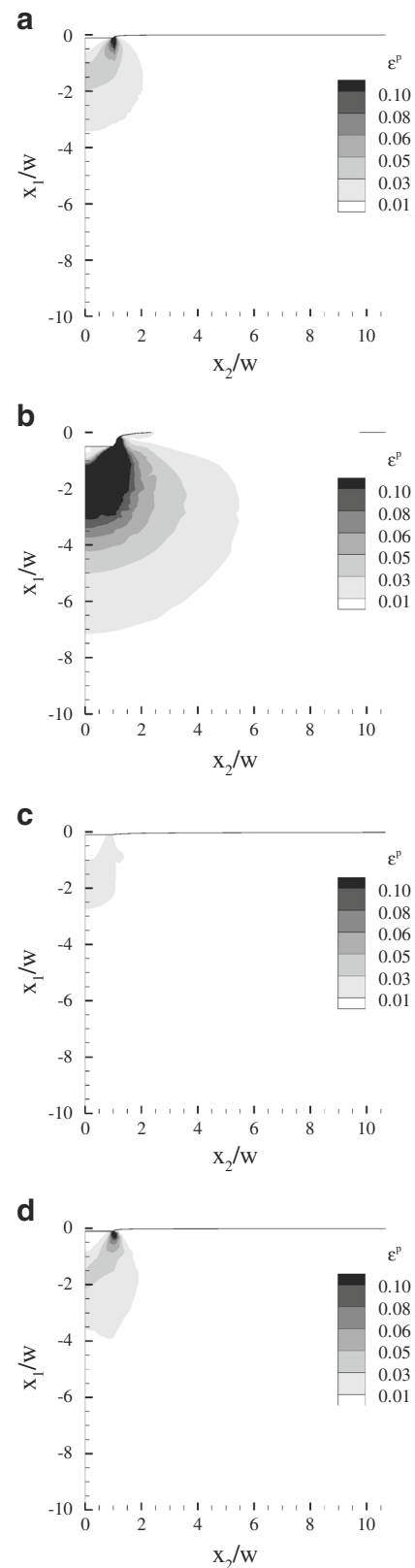

Fig. 3 Contour plots of ϵ^p for conventional plastic material (**a, b**) and for gradient plastic material (**c, d**). The value of $h/w = 0.1$ for (**a, c, d**) whereas $h/w = 0.5$ for (**b**). In case of the gradient plastic materials $w/l_* = 5$ and 20 for (**c, d**) respectively
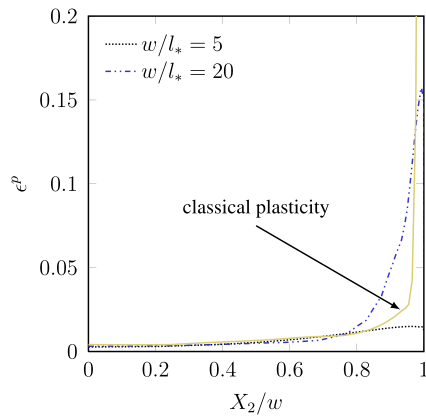
Fig. 4 Distribution of ϵ^p with X_2/w at $h/w = 0.1$

distribution of $\epsilon^p(X_2/w)$ for the classical case is independent of the punch width. Moreover, it is uniform over the punch face except near the sharp corner, where it rises steeply.

In case of the wider punch with $w = 20l_*$, the distribution of plastic strain over its face shows a variation similar to the classical case except for the fact that the sharp rise at the corner $X_2/w = 1$ is less severe. This is because strain gradient plasticity acts to smear out sharp variations in plastic strain and to some extent, mitigates the severe strain concentration at the corner. The effect is more dramatic for the punch with $w = 5l_*$ where the plastic strain is almost uniform over the whole face of the punch and the concentration at the corner is completely smeared out. This is also evident in the contours of ϵ^p in Fig. 3c.

The difference in the shapes of the plastic zones beneath a narrow and a wide punch is central to understanding the w dependence of H. This is further delineated by Figs. 5a through b. In Fig. 5, the contours of an effective measure of strain gradient (or the density of GNDs) has been shown for two punch widths. We use the quantity

$$||\nabla \epsilon^p|| = \left[\left(\epsilon^p_{,1} \right)^2 + \left(\epsilon^p_{,2} \right)^2 \right]^{1/2}, \tag{55}$$

in these plots. For the narrower punch, very high effective strain gradients are concentrated at the edge of the punch while the concentration is weaker for the wider punch. In fact, the uniformity in the distribution of ϵ^p is achieved at the cost of generating the high gradients of strain which, in turn, suggest a situation like that shown in Fig. 6—the indentation with the flat punch is accomodated by the generation of GNDs consisting of a wall of edge dislocations at the corner.

Indirect confirmation of the above observation is found in the experiments of Chen et al. [1]. Transmission Electron Microscopy of their molded sample shows the formation of nano-scale grains around the corner of the molded trench in the originally single crystal Al substrate. Moreover, the tilt
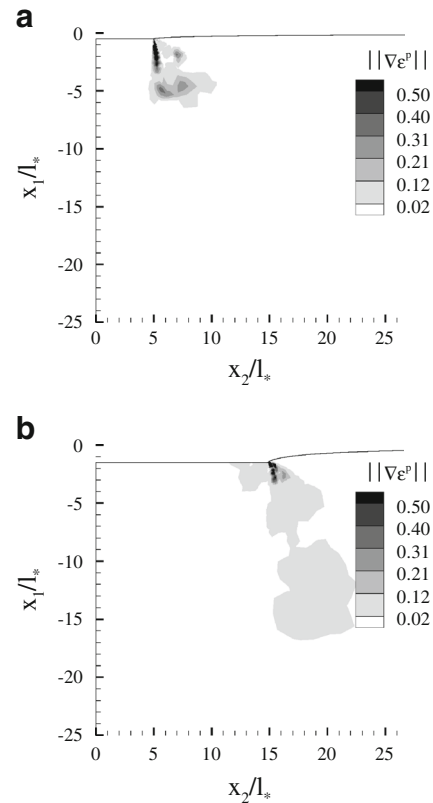

Fig. 5 Contours of $||\nabla \epsilon^p||$ for $h/w = 0.1$ and for **a** $w/l_* = 5$ and **b** $w/l_* = 15$

boundary between these nano-scale grains were found to be very small, typically less than 15°. Low angle boundaries can be assumed to be represented by collection of dislocations. This indirectly indicates that high dislocation density exists close to the edges in samples molded with narrow punches. Moreover, Chen et al. [1] found that the dislocation density within the specimen was relatively low, lending credence to the numerical observations of the previous paragraph.

Finally the contact stress σ_t, defined as $\sigma_t = -\sigma_{11}$ at $X_1 = 0$, is plotted in Fig. 7 as a function of X_2/w. It should be noted that this stress does not represent the hardness of the substrate material. For comparison, the contact stress
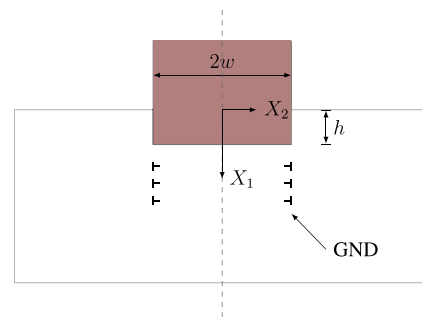

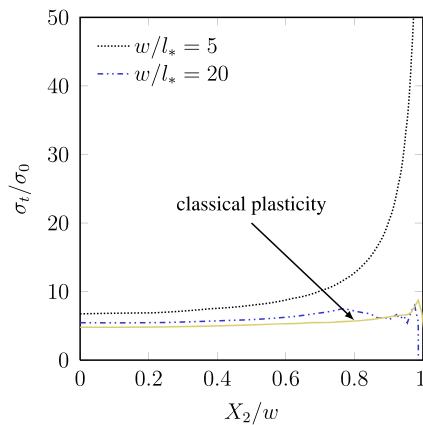**Fig. 6** Schematic of geometrically necessary dislocations under flat punch

Fig. 7 Variation of σ_t/σ_0 with X_2/w at $X_1 = 0$ for $h/w = 0.1$

expected from a conventional plasticity solution is also provided in this figure by solid line. The contact stress remains constant over the punch face in classical plasticity as well as for the case with the wider punch. However, for the narrow punch, high strain gradient at the corner of the punch leads to extremely high value of σ_t. While over most part of the punch the value of contact stress is almost constant and close to that predicted by classical plasticity, the dramatic rise in σ_t at the corner of the narrow punch leads to the high value of the molding pressure H experienced by the punch when its width is small. As w increases the severity of the gradient as well as of σ_t diminishes leading to lower H.

Conclusions

Chen et al. [1] have conducted experiments on flat punch molding of Al substrates and shown that the characteristic pressure H beneath the punch is much higher for narrower punches. We have conducted numerical simulations based on a higher order strain gradient theory to show that the dependence of H on the punch width w can be effectively captured. Moreover, we have demonstrated that the plastic zone beneath a very narrow punch is significantly different from that beneath a wide one. This difference holds the key to explaining why a narrow punch experiences a higher molding pressure.

In case of a punch with small width, high gradients of plastic strain are generated at the sharp corners leading, unlike in wider punches, to a uniform distribution of plastic strain. However, the high plastic strain gradients (which in turn implies the formation of a wall of edge dislocations at the edge) also lead to large values of contact stress near the corners and a high molding pressure H.

References

1. Chen K, Meng WJ, Mei F, Hiller J, Miller DJ (2011) From micro- to nano-scale molding of metals: size effect during molding of single crystal al with rectangular strip punches. Acta Mater 59:1112–1120. doi:10.1016/j.actamat.2010.10.044
2. Hill R (1950) The mathematical theory of plasticity. Oxford University Press, Oxford
3. Nepershin RI (2002) Indentation of a flat punch into a rigid-plastic half space. J Appl Math Mech 66:135–140
4. Lee CH, Kobayashi S (1970) Elastoplastic analysis of plane-strain and axisymmetric flat punch indentation by the finite-element method. Int J Mech Sci 12:349–370
5. Murthy TG, Huang C, Chandrasekar S (2008) Characterization of deformation field in plane-strain indentation of metals. J Phys D Appl Phys:41
6. Cao DM, Guidry D, Meng WJ, Kelly KW (2003) Molding of pb and zn with microscale mold inserts. Microsyst Technol 9:559–566
7. Cao DM, Meng WJ (2004) Microscale compression molding of al with surface engineered liga inserts. Microsyst Technol 10:662–670
8. Jiang J, Mei F, Meng WJ (2008) Fabrication of metal-based high-aspect-ratio microscale structures by compression molding. J Vac Sci Technol A 26:745–751
9. Madou MJ (1997) Fundamentals of microfabrication. CRC Press
10. Cross GLW, O'Connell BS, Pethica JB, Rowland H, King WP (2008) Variable temperature thin film indentation with a flat punch. Rev Sci Instrum 79(1):013904. doi:10.1063/1.2830028
11. Nix WD, Gao H (1998) Indentation size effects in crystalline materials: a law for strain gradient plasticity. J Mech Phys Solids 46:411–425
12. Fleck NA, Hutchinson JW (1997) Strain gradient plasticity. Adv Appl Mech 33:295–361
13. Fleck NA, Hutchinson JW (2001) A reformulation of strain gradient plasticity. J Mech Phys Solids 49(10):2245–2271. doi:10.1016/S0022-5096(01)00049-7
14. Swadener JG, George EP, Pharr GM (2002) The correlation of the indentation size effects measured with indenters of various shapes. J Mech Phys Solids 50:681–694
15. Aifantis EC (1984) On the microstructural origin of certain inelastic models. J Eng Mater 106:326–330
16. Stölken JS, Evans AG (1998) A microbend test method for measuring the plasticity length scale. Acta Mater 46:5109–5115
17. Fleck NA, Muller GM, Ashby MF, Hutchinson JW (1994) Strain gradient plasticity: theory and experiment. Acta Metall Mater 42:475–487
18. Borg U, Niordson CF, Fleck NA, Tvergaard V (2006) A viscoplastic strain gradient analysis of materials with voids or inclusions. Int J Solids Struct 43:4906–4916
19. Niordson CF, Redanz P (2004) Size-effects in plane strain sheet-necking. J Mech Phys Solids 52:2431–2454
20. De Borst R, Pamin J (1996) Some novel developments in finite element procedures for gradient-dependent plasticity. Int J Numer Methods Eng 39:2477–2505
21. Mikkelsen LP, Goutianos S (2009) Suppressed plastic deformation at blunt crack-tips due to strain gradient effects. Int J Solids Struct 46:4430–4436
22. Evans AG, Hutchinson JW (2009) A critical assessment of theories of strain gradient plasticity. Acta Mater 57:1675–1688
23. Tan T-M, Li S, Chou PC (1990) Finite element solution of prandtl's flat punch problem. Exp Syst Appl 1(1):173–186. ISSN 0957-4174
24. Riccardi B, Montanari R (2004) Indentation of metals by a flat-ended cylindrical punch. Mater Sci Eng A-Struct 381:281–291